Saudi Pharmaceutical Journal 28 (2020) 1035–1048

Contents lists available at ScienceDirect

Saudi Pharmaceutical Journal

journal homepage: www.sciencedirect.com

Original article

Sennoside A drug capped biogenic fabrication of silver nanoparticles and their antibacterial and antifungal activities

Areej Dhawi Al-Ghamdi, Zoya Zaheer *, Elham Shafik Aazam

Department of Chemistry, Faculty of Science, King Abdulaziz University, P.O. Box 80203, Jeddah 21589, Saudi Arabia

ARTICLE INFO

Article history:
Received 16 April 2020
Revised 5 June 2020
Accepted 1 July 2020
Available online 6 July 2020

Keywords:
Sennoside A
Silver nanoparticles
Green synthesis
Antioxidant
Antimicrobial

ABSTRACT

Sennoside A (dianthrone glycoside) shows laxative properties and used as a folk traditional medicine. Sennoside A capped silver nanoparticles (Ag/sennoside A) were synthesized at room temperature for the first time by using sennoside A as reducing and capping agent. UV–visible spectroscopic data reveals that the absorption peaks of pure sennoside A was appeared at 266, and 340 nm, which red shifted to 304, and 354 nm at higher sennoside A concentration. Upon addition of the Ag^+ ions, an additional peak also observed at 398 nm, indicating the formation of spherical sennoside A capped silver nanoparticles (Ag/sennoside A). Cetyltrimethylammonium bromide (CTAB) was used a stabilizing agent to determine the role of cationic micelles on the nucleation and growth processes of Ag/sennoside A NPs formation. The 2,2-diphenyl-1-picrylhydrazyl nitrogen radical ($DPPH^{\cdot}$), two bacteria strains (Staphylococcus aureus and Escherichia coli) and two yeast strains (Candida albicans ATCC 10231 and Candida parapsilosis ATCC 22019) were used to determine the antioxidant and antimicrobial properties of Ag/sennoside A NPs. In addition, Rhein-9-anthrone (4,5-dihydroxy-10-oxo-9*H*-anthracene-2-carboxylate) was isolated from the acidic hydrolysis of glycoside linkage of sennoside A and characterized. The antioxidant and antimicrobial activities of rhein-9-anthrone were also determined against DPPH radical, antibacterial and antifungal strains. The minimum inhibitory concentration was determined and discussed.

1 Introduction

Plants raw materials have been used widely as drug for medicinal practice to cure the human health disorder of various systems from ancient time (Sendelbach, 1989). Due to their potential pharmacological and therapeutic application, the natural plants extract have been widely used in cosmetics, food, dye and pharmaceuticals industries (Mueller et al., 1999; Yen et al., 2000). For example, the anthracene derivatives are one of the most important drugs used as laxative in the treatment of digestive disorder and anthropoids (Hattori et al., 1982; British Pharmacopoeia, 1999; Dave and Ledwani, 2012). Cassia Linn. (belongs to Caesalpiniaceae family) is a herb of many species and has various medicinal constituents. Cassia (senna leaves) are the main source of anthraquinones and its derivatives. Leaves, seeds and roots of all species are used in folk medicine. Senna leaves contained many quinonids, dianthrone glycosides, sennosides, hydroxylated anthraquinones, glycosides, anthraquinone dyes, and others (Dave and Ledwani, 2012; Tyler et al., 1988). Out of these, sennosides are the major constituents of senna leaves (*Cassia angustifolia*) and their structures are given in Scheme 1.

Silver and its NPs are nontoxic, ecofriendly and safe inorganic antimicrobial agent and has capability to kill diseases causing microorganisms from centuries. The noble silver metal NPs have sharp absorption peak in the UV–visible region from 350 to 650 nm (Henglein, 1993, 1998; Mulvaney, 1996; Saeb et al., 2014) due to the surface plasmon resonance (SPR) band. Silver NPs were extensively used in various applications such as biosensing (Haes and Duyne, 2002), environmental fortification (Choi et al., 2008), drug-delivery (Paula, et al., 2009), medicinal products (Eby et al., 2009), food diet (Kon et al., 2014), catalysis (Hayelom et al., 2017), water purification (Khan et al., 2018), detection of cancer (Huy et al., 2019), and sensors (Khan, 2019). The morphology depends on the presence of stabilizer, method of synthesis, and nature of reducing agent (Henglein, 1993, 1998; Mulvaney, 1996; Sharma et al., 2009). The presence of a suitable

* Corresponding author.
E-mail addresses: zoya.zaheer@gmail.com, zzkhan@kau.edu.sa (Z. Zaheer).
Peer review under responsibility of King Saud University.

Production and hosting by Elsevier

https://doi.org/10.1016/j.jsps.2020.07.003
1319-0164/

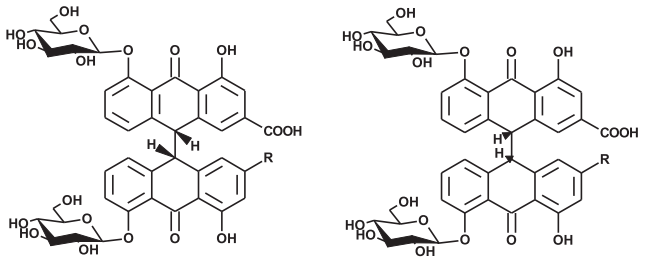

Scheme 1. Structure of sennosides (cassia angustifolia).

stabilizer is essential to block the unlimited growth, precipitation and agglomeration. Generally, surfactant, polymer, carbohydrates, proteins, copolymer, lipids, natural plants extract were used as a capping agent. Out of these, an aqueous plant extract have superiority over the other stabilizers. The constituents of extract such as, water soluble biomolecules, flavonoids, glycosides, tannic acid, polyhydroxy phenols, betanin and others acted as a reducing and stabilizing agent. They eliminate the necessity of the externally added toxic stabilizer (Ahmad and Sharma, 2012; Hussain and Khan, 2014; Rafique et al., 2017).

Existing literature contained abundant reports successful fabrication of AgNPs through green route using azadirachta indica (Shankar et al., 2004), chlorella vulgaris (Xie et al., 2007), acalypha indica (Krishnaraj et al., 2010), anacardium occidentale (Sheny et al., 2011), piper betel (Khan et al., 2012), mentha leaves (Zaheer et al., 2016), ferula persica (Nasiri, et al., 2018), palm date fruit (Zaheer, 2018), zingiber officinale (Eisa, et al., 2019), water soluble starch (Khan, 2019), and betanin (Kosa and Zaheer, 2019). Generally, the presence of a suitable stabilizer is essential to block the unlimited growth and aggregation of NPs. Surfactant, polymer, ligand, and organic solvents were used as a capping agent. Cetyltrimethylammonium bromide (cationic surfactant) acted as an excellent stabilizing agent in the nanotechnology, which can be removed from the surface of NPs by washing (Bakshi, 2009; 2016; 2018). Systematic synthesis of AgNPs using sennoside A has been neglected. Sennosides and anthracene derivatives have been used as laxative to the treatment of constipation and colon infection. Therefore, we used sennoside A as a reducing agent to the synthesis of AgNPs for the first time.

Our goal of this study was to fabricate biogenic AgNPs by using sennoside A as a reducing agent in absence and presence of shape directing and controlling cationic aggregates of CTAB. The antioxidant activities of sennoside A, and Ag/sennoside A were determined by using DPPH radical. Bacterial (Staphylococcus aureus and Escherichia coli) and yeast strains (Candida albicans ATCC 10231 and Candida parapsilosis ATCC) were used to the evaluation of antimicrobial activities of as prepared AgNPs against standard gentamicin and fluconazole. These studies would enhance the medicinal significance of the individual components such as sennoside A and metallic silver. We also focused on isolation and characterization of rhein-9-anthrone (4, 5-dihydroxy-10-oxo-9*H*-anthracene-2-carboxylate) from acidic hydrolysis of sennoside A, which was the main constituent responsible to prevent the colon infection (van Gorkom et al., 2001).

2. Experimental section

2.1. Chemicals

Cetyltrimethylammonium bromide ($C_{19}H_{42}NBr$, molecular weight = 364.45 g/mol), silver nitrate ($AgNO_3$, molecular weight = 169.87 g/mol), safranin ($C_{20}H_{19}N_4^+.Cl^-$, molecular weight = 350.85 g/mol, water soluble) were purchased from Sigma-Aldrich and there stock solutions were prepared in deionized water by molarities basis. All chemicals inorganic electrolytes (NaCl, NaBr, NaI, $NaNO_3$, Na_2SO_4 and NaOH), organic solvents (methanol, ethanol, chloroform, and diethyl ether) and HCl were of analytical grade. Water (deionized and CO_2 free) was employed as solvent for the preparation of solutions and dilution. Standard HCl and NaOH solutions were used to maintain the pH for the batch kinetic experiments. Silver nitrate solution was kept in dark to minimize the photochemical oxidation. The deionized water was used as solvent throughout the studies.

2.2. Extraction of sennoside A

The fresh leaves of senna (*Cassia angustifolia* Del.) were collected from the garden of our science college (female section, King Abdulaziz University) and authenticated by Dr. Majid, Department of biology, Faculty of Science, King Abdulaziz University, Jeddah. The leaves were washed thoroughly under water widely and finally with double distilled water to remove dust particles and other foreign materials. In a typical experiment, 10 g dried senna leaves were added in a stoppered conical flask containing 200 ml double distilled and heated at 80 ^{0}C constant temperature water bath for 30 min with constant stirring. The extract cooled at room temperature and filtered with a Whatman filter paper to remove the leaves wastes. The resulting fresh extract was used to obtain the solid sennoside A by using rotatory evaporator (EYELA rotatory evaporator N-1300E.V.S series, Tokyo, Japan) under vacuum at 80 ^{0}C temperature. A dark yellow compound was obtained.

The aqueous extract of senna leaves contains sennosides (A and B), aloe-emodin (glycoside and diglycoside) and rehin (glycoside, diglycoside, and anthrone) (Sun and Su, 2002). Habib and Elsebakhy reported that the UV–visible spectra of aloe-emodin and rehin showed a well-defined sharp absorption peak at ca. 260 nm and 440 nm and sennosides A and B exhibited absorption peak at 270 nm and 370 nm in ethylacetate (Habib and Elsebakhy, 1980). Tan et al. reported that the standard solution of sennoside A and sennoside B showed absorption peaks at 269 nm, 340 nm and 268 nm and 358 nm, respectively, in water-acetonitrile system (Tan et al., 2015). They also suggested that the separation of both isomers from each other were also difficult. In order to characterize the extracted dark yellow solid, UV– visible spectra were recorded under different experimental conditions. Our spectra does not contained any absorption peak in the entire visible region (Fig. 1; vide infra), which indicated that the aloe-emodin and rehin constituents were not present in the aqueous extract. On the other hand, the absence of absorption peaks at 358 nm also indicated that the sennoside B was also not present in the extract and was ignored completely. Therefore, sennoside A was the main constituent in the aquous extract and its molar concentration was calculated with using molar extinction coefficient, ε = 9430 L/mol/cm (Hietala et al., 1988) at 340 nm wavelength. The Beer-Lambert law was obeyed for the entire range concentration (from 1.0×10^{-4} to 18.0×10^{-4} mol/L) of sennoside A with correlation coefficient (R^2 = 0.998).

2.3. Fabrication of Ag/sennoside A NPs

Sennoside A drug was used as a reductant to the reduction of Ag^+ ions for the fabrication of AgNPs. In a typical experiment, sennoside A (1.4×10^{-4} mol/L) was added drop-wise in a conical flask containing 5 ml aqueous solution of $AgNO_3$ (0.01 mol/L; total volume = 40 ml) under constant stirring with a help of a magnetic stirrer at 1500 rpm for 30 min. The appearance of yellow, orange to dark brown colors was indicated the reduction of Ag^+ ions into

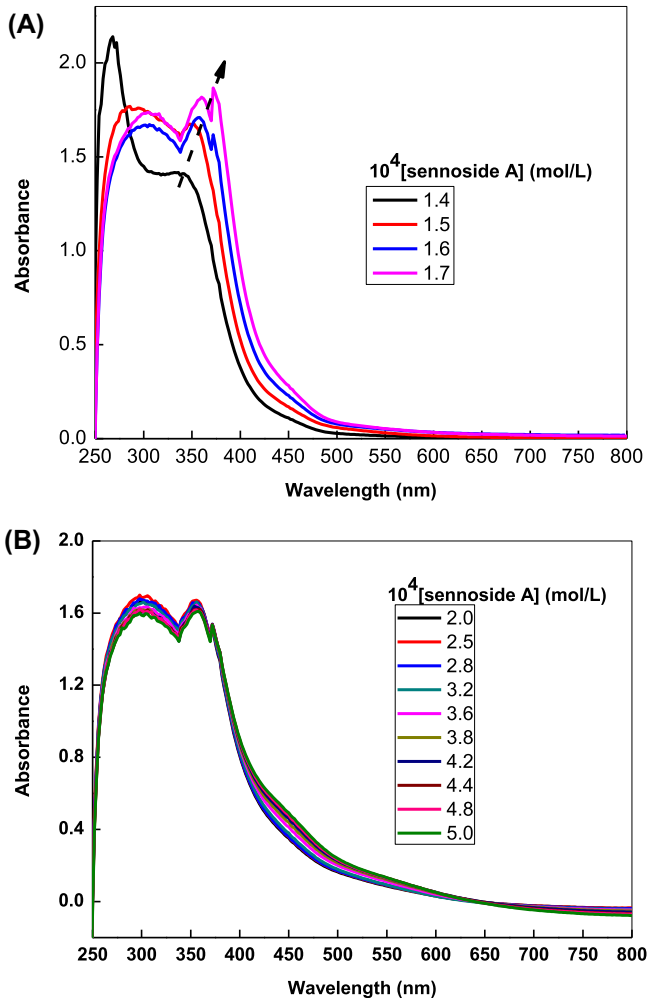

Fig. 1. UV–visible spectra of sennoside A at lower (Fig. 1A) and higher concentrations (Fig. 1B) extracted from senna leaves with hot water. *Reaction conditions*: senna leaves = 10 g, and solvent = hot water.

metallic silver (Ag^0). The resulting brown red color was centrifuged for 30 min with 15 000 rpm at 298 K. The obtained solid AgNPs were dried at 353 K and stored in dark condition at room temperature. In the next experiment, same sennoside A solution was added in a mixture of $AgNO_3$ and CTAB (0.073 g, 0.02 mmol) to determine the effect of CTAB on the Ag/sennoside A. Optical images of reaction mixture containing sennoside A, Ag^+ and CTAB are given in Scheme 2 at different time intervals.

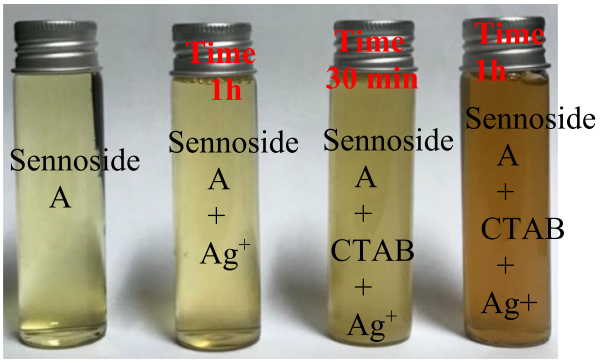

Scheme 2. Effect of time on the reduction of Ag^+ by sennoside A.

2.4. Characterization of Ag/sennoside A

The UV–visible spectra of extracted sennosides were recorded by using Shimadzu UV-260 spectrophotometer. The shape, size and the size distribution (the surface morphology) of Ag/sennoside A were determined with UV–visible spectroscopy, scanning electron microscope (SEM), transmission electron microscope (TEM, JEM 2100), equipped with energy dispersed X-ray detector (EDX), X-ray diffraction spectroscopy (XRD), dynamic light scattering (DLS) and zeta potential. The specific surface area of these NPs was estimated from nitrogen adsorption–desorption isotherms (Brunauer-Emmett-Teller; BET) by using Quantachrome Nova 3200e Surface area & pore size analyzer, Instrument. For TEM measurement, silver sol was deposited on a carbon coated copper grid, dried at room temperature under open air. The X-ray photoemission spectroscope (XPS) was used to determine the chemical and electronic state of silver by using XSAM-800 m featuring a monochromatic Mg Kα X-ray source at 21.5 mA with $h\nu$ = 1486.6 eV.

2.5. Determination of anti-radical scavenging activity

The DPPH radical solution (0.001 mol L^{-1}) was prepared in methanol. The 2.0 cm^3 radical solution was mixed with 5.0 cm^3 of sennoside A (1.4×10^{-4} mol/L) at 30 °C. The antioxidant efficiency was measured at 517 nm (λ_{max} of DPPH radical) as a function of time. The ascorbic acid was used as controls. The percentage of DPPH scavenging activity was determined by using the Eq. (1). All measurements were made in triplicate.

$$\%DPPH\,activity = \left[\frac{1-(absorbance\,of\,sample - absorbance\,of\,bank)}{absorbance\,of\,control}\right] \times 100 \quad (1)$$

2.6. Antimicrobial activity

The agar diffusion dilution essay method was used for the estimation of antibacterial and antifungal activities of sennoside A, biosynthesiszed Ag/sennoside A NPs and rhein-9-anthrone (Abraham et al., 1941). Two bacterial strains, namely, *Staphylococcus aureus* ATCC 25923), and *Escherichia coli ATCC 25922* and two reference yeast strains (*Candida albicans ATCC 10231* and *Candida parapsilosis ATCC 22019*) were used for this purpose. In a typical experiment, the sterile disks were loaded with required concentration of test samples and then placed on agar plate containing strain lawns and incubated at 310 K temperature for 24 h. The zones of inhibition for reference, negative control, and test samples were measured from the diameter (mm) of the clear zone. The minimum inhibitory concentration (MIC_{50}) was estimated according to the reported method for various AgNPs concentrations. Gentamicin and fluconazole were used as a reference compound for antibacterial and antifungal activities, respectively. Three independent experiments were carried out for each target samples.

3. Results and discussion

3.1. Preparation method and reaction mechanism of Ag/sennoside A NPs

3.1.1. UV–visible spectroscopic studies of sennoside A

Fig. 1A shows the resulted aqueous extract of sennoside has two absorption peaks at λ_{max} = 266 and 340 nm. No absorption peak was appeared at 358 nm (Fig. 1), which ruled out the presence of sennoside B and other chemical constituent in our extracted sennoside from *Cassia angustifolia*. Our values of λ_{max} are in good

agreement with the λ_{max} of standard sennoside A reported in the literature (Tan, et al., 2015). The sennoside A concentration was calculated by the reported method with molar extinction coefficient, ε = 9430 L/mol/cm (Hietala, et al., 1988). Interestingly, the peak intensity decreases and red shifted from 266 nm to 288 nm with increasing sennoside A concentrations from 1.4×10^{-4} to 5.8×10^{-4} mol/L at a fixed temperature, whereas the peak intensity increases and red shift was also observed from 340 nm to 374 nm, indicating the J-type aggregation of sennoside A molecules to each other (Mas-Montoya and Janssen, 2017). Such type of behaviors was not observed at higher sennoside concentrations (Fig. 1B). The peak position remains constant with [sennoside A]. The peak position at 266 nm might be due to the π-π* and n-π* transitions of –OH and carbonyl groups in the sennoside A. Our position of peaks are in good agreement with results of other investigators regarding the UV–visible spectra of substituted anthraquinons, which shows intense quinonoide peak in the vicinity of 260 to 290 nm (Thomson, 1971). The FTIR spectrum of sennoside were recorded and the various peak at 3430, 2930, 1610, 1520, 1050 cm^{-1} were observed, which can be attributed to the presence of –OH groups, C-H stretching, C = O group (or OH from –COOH), C = C benzene ring and C-O stretching, respectively (Fig. not given). Thus we may state confidently that our extracted dark yellow solid has sennoside A in the greatest concentration (Sun and Su, 2002; Tan, et al., 2015).

3.1.2. Effect of [Ag^+]on the SPR of AgNPs

In order to establish the role of sennoside A as a reducing agent, a series of kinetics experiments were performed by varying [Ag^+] from (0.5×10^{-3} to 2.5×10^{-3} mol/L) at a fixed concentration of sennoside A = 1.4×10^{-4} mol/L (Table 1). Fig. 2 shows that the intensity and position of peaks depends on the [Ag^+]. For example, at lower [Ag^+], peak intensity at 266 nm decreases with reaction time, whereas the absorbance of 340 nm peak increases, attaining maximum absorbance and decreases as a function of time, indicating the interaction of sennoside A with Ag^+ ions and optimum concentration of Ag^+ ions required to form stable AgNPs (Fig. 2A). Fig. S1A, S1B and S1C (supporting information) indicates that the lower and higher [Ag^+] (0.5, 1.2, and 2.5×10^{-3} mol/L) are not suitable to the kinetic experiments. At [Ag^+] = 0.7×10^{-3} mol/L, the both λ_{max} of sennoside are red shifted from 266 to 290 nm and 340 to 352 nm (Fig. 2B). Interestingly, a new peak and a broad shoulder at 385 and 450 begin to develop as a function of time, suggesting the reduction of Ag^+ into Ag^0 (Raveendran et al., 2003), silver sols formation. It is well known that the yellow color of aqueous silver sols exhibited in intense SPR band in the UV–visible region from 350 to 650 nm. The shape and position of SPR band depends on the experimental conditions such as presence of solvent, nature of reducing agent, capping action of stabilizer and chemisorbed solute molecules (Henglein, 1993, 1998; Mulvaney, 1996). The stability of NPs was determined by keeping the silver sols at 30 °C for different day intervals. The resulting silver sols were perfect transparent for ca. one week. We did not observe the appearance of any type of precipitate or turbidity. The optical properties of AgNPs depend on the nature of stabilizer and capping agent present in the reaction mixture. The SPR band intensity was diminished due to the adsorption of sennoside A onto the surface of metallic silver (Henglein, 2000; Mulvaney, 1996).

Table 1
Effects of [sennoside A], [Ag^+] and [CTAB] on the stability and SPR of Ag/Sennoside A at 298 K.

[Sennoside A] (mg/L)	[Ag^+] (mg/L)	[CTAB] (mg/L)	SPR, stability, color, λ_{max} of AgNPs
120.78	0.0	0.0	No SPR intensity of AgNPs
120.78	75.5	0.0	Pale yellow, stable, 385, 450 nm
215.68	75.5	0.0	Pale yellow, stable, 385, 450 nm
500.39	75.5	0.0	Yellow, stable, 385, 450 nm
120.78	53.9	0.0	Pale yellow, stable, no SPR
120.78	269.6	0.0	Pale yellow, stable, 385, 450 nm
120.78	75.5	184.2	Yellow, stable, no SPR
120.78	75.5	460.5	Yellow, stable, 395 nm, 450 nm
120.78	75.5	921.1	Yellow, stable, 395 nm, 450 nm
43.13	75.5	460.5	Pale yellow, turbidity
215.68	75.5	460.5	Orange, stable, 395 nm, 450 nm
301.94	75.5	460.5	Orange, stable, 395 nm, 450 nm
500.39	75.5	460.5	Yellow precipitate after 20 min

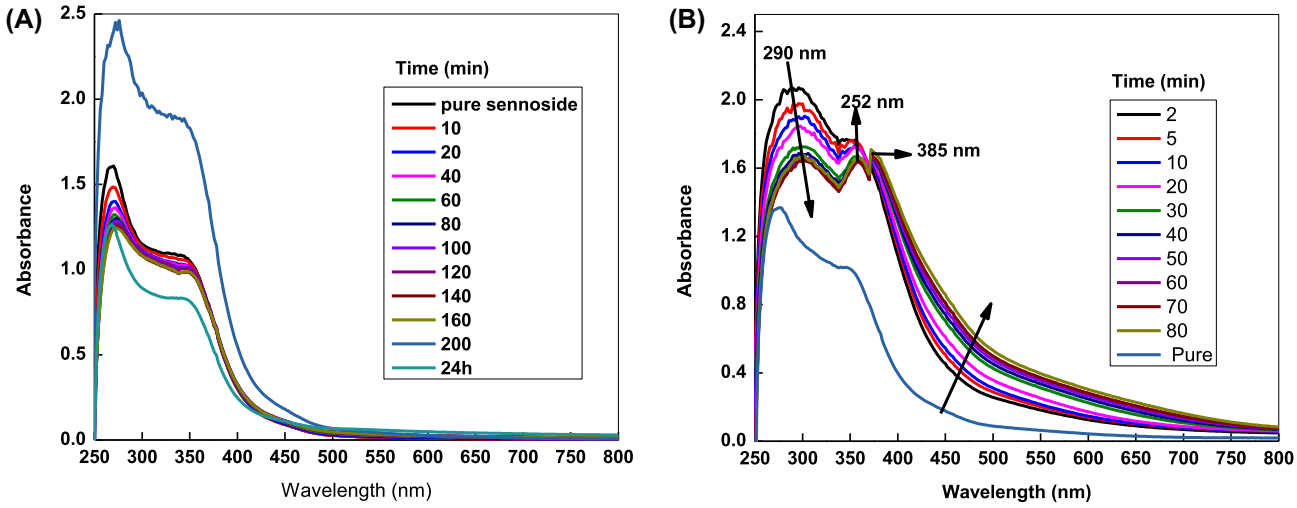

Fig. 2. UV–visible spectra of Ag/sennoside A NPs. *Reaction conditions*: [sennoside A] = 1.4×10^{-4} mol/L, [Ag^+] = 0.6 (A), and 0.7×10^{-3} mol/L (B).

3.1.3. Effect of CTAB

Stabilizer has significant impact on the morphology of advanced nano-materials. They increased and decreased the nucleation rate by solubilizing the reactants as well as the products. Therefore, effect of CTAB from 2.0×10^{-4} to 25.0×10^{-4} mol/L was studied on the redox reaction of sennoside A ($=1.4 \times 10^{-4}$ mol/L) and Ag^+ ($=0.7 \times 10^{-3}$ mol/L) at 298 K (Table 1). The lower ($=2.0 \times 10^{-4}$ mol/L) and higher ($=25.0 \times 10^{-4}$ mol/L) concentrations of CTAB was not suitable to the formation of stable AgNPs (Fig. 3) due to the sub and dilution-micellar effect of CTAB aggregates. At 12.5×10^{-4} mol/L [CTAB], the absorbance increases of both peaks and 266 nm peak is red shifted to 304 nm (total shift 38 nm). The absorbance at 395 nm initially increases, then decreases with increasing time and stabilized (Fig. 3A). Finally, resulting silver sol shows three absorption bands at 304, 358 and 395 nm. Presence of sennoside A peaks along with a surface resonance plasmon band of Ag^0, suggesting the formation of Ag/sennoside A under our experimental conditions. Inspection of Fig. 3, clearly indicates that the nucleation and growth was governed by the CTAB aggregates, which might be due to the sub- and post-micellar effect of CTAB with sennoside A. Fig. 3A indicated that the Ag/sennoside A shows the presence of two absorption peaks at 304 and 358 nm (red shifted from 266 and 340 nm), which originally come from the sennoside A. Thus it is confirmed that Ag_4^{2+} -sennoside A system behaves as J- aggregates (Mas-Montoya and Janssen, 2017).

Inspection of Figs. 2 and 3 clearly indicated that the UV–visible spectra of pure sennoside A, Ag/Sennoside A NPs and CTAB capped Ag/Sennoside A NPs were quite different to each other. The intensity and position of SPR band strongly depends on the [Ag^+] and [CTAB]. The absorption peaks of pure sennoside A at 266 and 340 nm were completely disappeared in presence of Ag^+ ions (Figs. 2B and 3A), indicating the complete oxidation of sennoside A by Ag^+ ions and stabilization of Ag^0 simultaneously. As a result, sennoside A acted as a reducing as well as capping agent, and leads to the formation of AgNPs. The capping action of oxidized sennoside A cannot be ruled out completely.

In order to establish the effect of sennoside A concentration on the nucleation and growth process of AgNPs formation, a series of experiments were performed with varying concentrations of reducing agent from 0.4×10^{-4} mol/L to 5.8×10^{-4} mol/L at fixed [Ag^+] = 0.7×10^{-3} mol/L , [CTAB] = 12.5×10^{-4} mol/L and temperature = 298 K. Table 1 shows that the lower and higher sennoside A concentrations were not suitable to the preparation of perfect transparent and stable silver sols. To determine to role of temperature, the reaction mixture containing sennoside A = 1.4×10^{-4} mol/L, [Ag^+] = 0.7×10^{-3} mol/L, and [CTAB] = 12.5×10^{-4} mol/L was heated at higher temperature from 303 to 323 K at constant temperature water bath. The visual observations indicated that the intensity of resulting yellow-orange silver sols increases with increasing the temperature. The sols were not stable and tur-

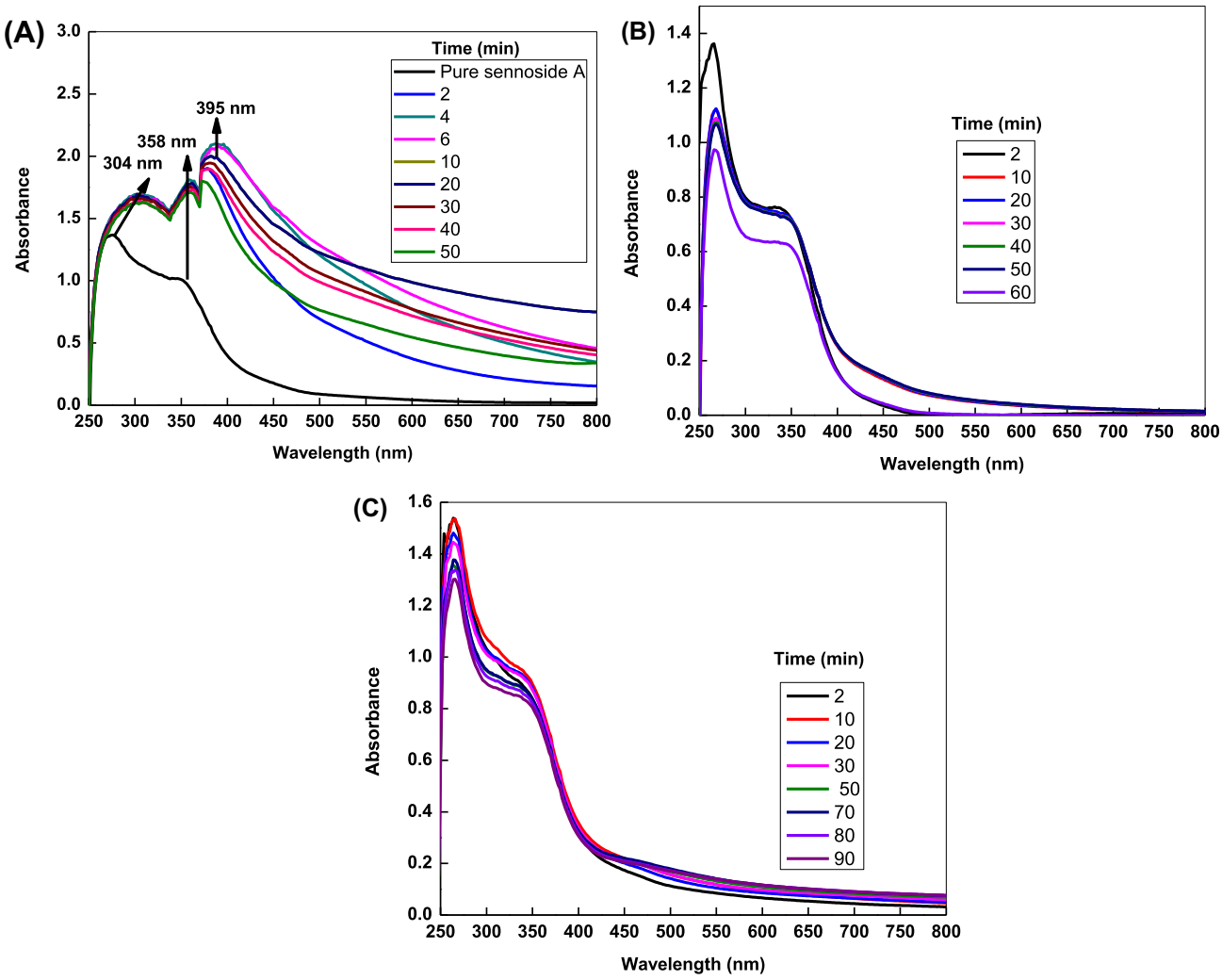

Fig. 3. UV–visible spectra of Ag/sennoside A NPs as a function of [CTAB]. *Reaction conditions*: [Sennoside A] = 1.4×10^{-4} mol/L, [Ag^+] = 0.7×10^{-3} mol/L, [CTAB] = 5.0 (A), 12.5 (B) and 25.0×10^{-4} mol/L (C).

bidity was appeared at higher temperature, which might be due to the agglomeration and /or uncontrolled growth of AgNPs.

The effects of NaOH (varying from 1.0×10^{-2} mol/L to 5.0×10^{-2} mol/L) was also studied with constant concentrations of oxidizing agent (0.7×10^{-3} mol/L), reducing agent (1.4×10^{-4} mol/L), CTAB (12.5×10^{-4}). The yellowish-white turbidity was appeared instead of transparent yellow-orange color (characteristic of AgNPs) with in 30 min of reaction time. To determine the effect of dissolved atmospheric molecular oxygen, the pure nitrogen gas was bubbled through the reaction mixture and UV–visible spectra were recorded. No significant spectral changes (shape, position and intensity of SPR band) were observed in the de-aerated resulting silver sols (Wojtysiak and Kudelski, 2012).

3.1.4. Mechanism and capping action of sennoside A

Sennoside A has various –OH groups such phenolic –OH, primary and secondary –OH of glucose. In order to establish the role of glucose –OH groups, some kinetic runs were performed by using glucose as a reducing agent instead of sennoside A. In a typical experiment, glucose (5.0 ml of 0.01 mol/L) added in a reaction vessel containing Ag^+ (5.0 ml of 0.01 mol/L), CTAB (5 ml of 0.01 mol/L) and water (25 ml) for dilution. We did not notice the appearance of any yellow to brown color within a short reaction time, i.e., 30 min, whereas, an absorption peak develops at 396 nm just after the mixing of sennosideA into the mixture of Ag^+ and CTAB (Fig. 3C). Thus phenolic –OH group of sennoside A are responsible for the fast reduction of Ag^+ into Ag^0. Thus, Scheme 3 mechanism is proposed for the reduction of Ag^+ by phenolic –OH group of sennoside A.

In Scheme 3, Eq. (2) represents the one-step redox reaction between phenolic –OH and Ag^+, which results to the formation of sennoside A radical and Ag^0. To detect the generation of radical, 5.0 ml acrylonitrile was added in the reaction mixture (Ag^+, sennoside A + CTAB). The white precipitate appeared as the reaction time increases, which confirmed in situ formation of corresponding free radical. In the next step (Eq.4), Ag^+ adsorbed on Ag^0 and Ag_2^+ was formed, which under goes dimerization, and leads to the formation of stable Ag_4^{2+} nano cluster (Henglein, 1993). To conform the presence of Ag^+ ions in the resulting silver sols, 5.0 ml of NaCl (0.1 mol/L) and NaBr (0.1 mol/L) solutions were added in a separate reaction flask. No white and yellow precipitates for AgCl and AgBr, respectively, were appeared, indicating the complete reduction (100%) of Ag^+ ions into Ag^0 and/or adsorption of Ag^+ onto the surface of Ag^0 (Henglein, 1993). The surface of Ag_4^{2+} species is positive and capped with sennoside A via –OH groups of glycoside through electrostatic interactions (Scheme 4).

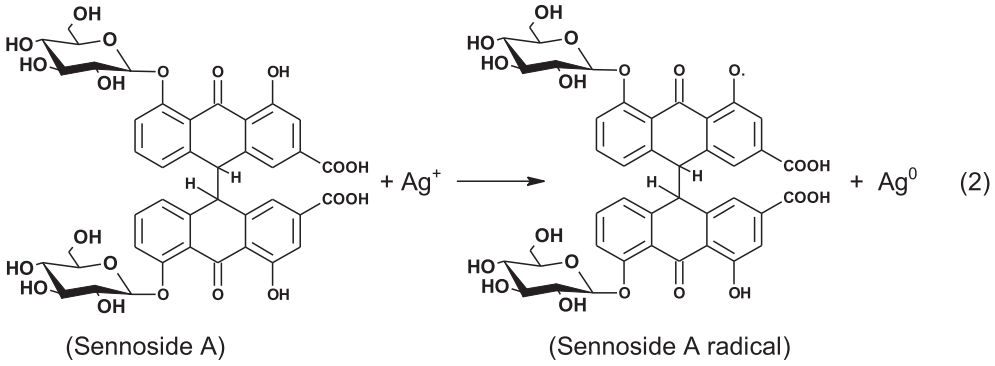

Scheme 3. Sennoside A assisted synthesis of AgNPs.

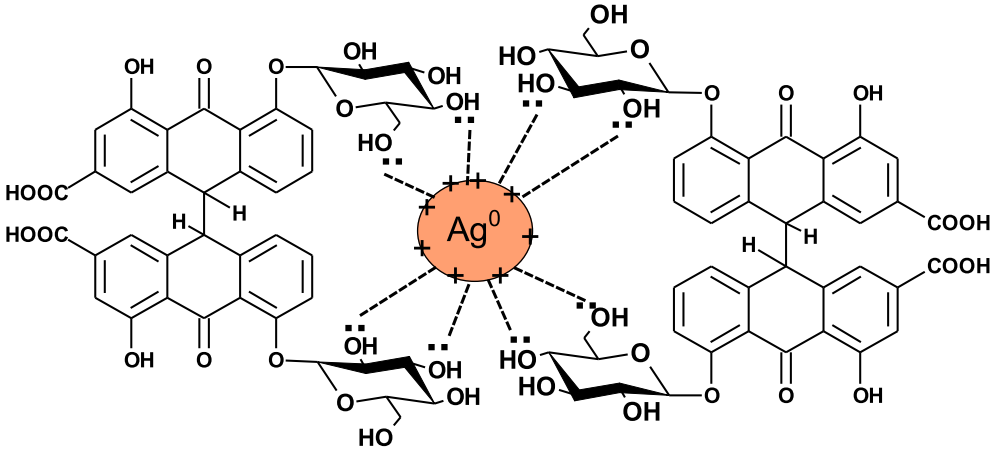

Scheme 4. Capping action of sennoside A towards AgNPs.

3.1.5. Morphology of sennoside A capped AgNPs

Fig. 4A shows the EDX of sennoside A capped AgNPs, which indicates the presence of only Ag element along with carbon and oxygen. The corresponding SEM and TEM images are given in Fig. 4B and C, respectively, which reveals the presence of roughly spherical well dispersed NPs. The size of NPs was calculated from the TEM images with Gaussian distribution and average particle diameter was found to be 12 nm (Fig. 4C). The size distribution histogram of NPs was prepared from the corresponding TEM image (Fig. 4C inset). Inspection of image clearly indicates that the presence of black spot on the surface NPs, which might be due to the capping properties of sennoside A (Shankar et al., 2004).

The surface zeta potential (ζ) provides information about the potential stability of colloid and decrease as a function of time due to the aggregation (Meléndrez, et al., 2010). For stable NPs the zeta potential values should be more positive than +30 mV and more negative than −30 mV (Saeb et al., 2014). Therefore, in order to determine the stability of as prepared Ag/Sennoside A, zeta potential were measured under different conditions by using Smoluchowski equation (Eq. (5)).

$$\zeta = \frac{4\pi\eta}{D} \times EM \tag{5}$$

where η, and D are the viscosity and dielectric constant of the solvent at the experimental temperature, respectively. The EM is the electrophoretic mobility. The zeta potential values were found to be −10 mV and −25 mV, respectively, for freshly prepared Ag/Sennoside A and CTAB capped Ag/Sennoside A, which indicating that the CTAB acted as a good stabilizing agent and provides higher stability to the resulting NPs (Bakshi, 2018). The stability of as prepared AgNPs were determined by recording the change in zeta potential for 7 days. The results of (ζ) versus time were plotted in Fig. 5, which indicates the CTAB capped Ag/Sennoside A NPs are more stable than that of Ag/Sennoside A NPs. The negative charges might be due to the adsorption of Sennoside A on the surface of formed AgNPs (Elemike et al., 2019).

The polydispersity index (PDI), which represents the distribution size population within a given sample and used for the acceptability of the AgNPs for biomedical and pharmaceutical applications such as antibacterial and antifungal (Raj et al., 2018). The numerical values PDI were ranges from 0 to 1.0 for a uniform mono-dispersed distribution and highly poly-dispersed particle size population. The hydrodynamic size distribution (z-average-size) and PDI of as prepared AgNPs were determined and found to be 18.2 nm and 0.6, respectively, indicating higher poly-dispersed.

In order to determine the crystalline nature of as prepared AgNPs, the XRD spectrum was recorded. The observed results are summarized in Fig. 6A. The diffraction four peaks appearing at 2θ = 33.00^0, 45.30^0, 64.10^0, and 80.20^0 correspond to the (1 1 1),

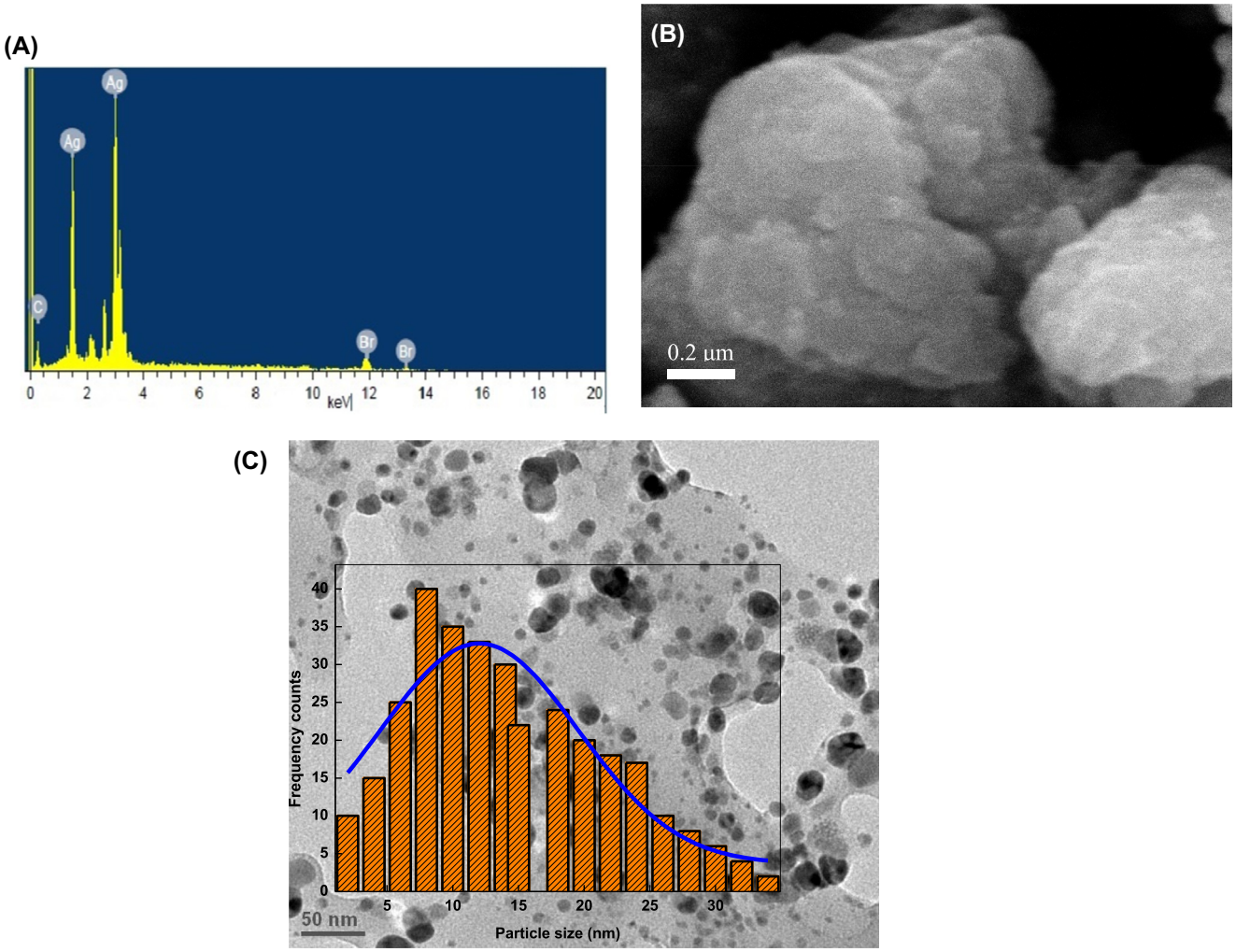

Fig. 4. EDX (A), SEM (B), TEM images along with particle size distribution histogram (C) of Ag/sennoside A NPs. *Reaction conditions*: [Sennoside A] = 1.4 × 10^{-4} mol/L, [Ag^+] = 0.7 × 10^{-3} mol/L, [CTAB] = 5.0 × 10^{-4} mol/L.

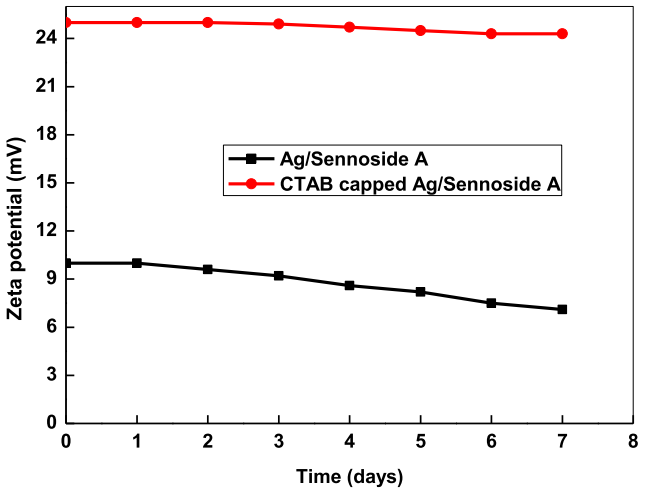

Fig. 5. Zeta potentials as a function of time for the Ag/Sennoside A and CTAB capped Ag/Sennoside A NPs. (Particle charge was negative for both samples).

(200), (220), and (311); JCPDS = 04-0783) facets of the face centered cubic structure of silver. The Scherrer formula was used to determine the crystallite size (D) of AgNPs (Eq. (6))

$$D = \frac{k\lambda}{\beta Cos\theta} \quad (6)$$

where D = average crystallite size, k = constant equal to one, λ = wave length of X-ray source (0.1542 nm), β = angular line full width at half maximum intensity in radians and θ = Braggs angle. The mean crystallite size was found to be 14.2 nm to the width of (111) and (220) diffraction peaks nearly in close agreement with the NPs size calculated from TEM image. The values of interplaner spacing (d) were calculated with Bragg's law (Eq. (7)).

$$d = \frac{n\lambda}{2\sin\theta} \quad (7)$$

For n = 1 order of reflection, d111 = 2.8 Å and d220 = 2.1 Å was calculated with Eq. (7).

XPS measurements were performed to identify the chemical and electronic structure of AgNPs. As shown in Fig. 6B, the most prominent signals at binding energies of 368.2 eV and 374.3 eV were corresponding to the $Ag3d_{5/2}$ and $Ag3d_{3/2}$ orbits of unperturbed metallic silver. The lower intensity peak at higher binding energy is attributed to the positively charged Ag atoms at the surface of the NPs (Wang et al., 2013). The binding energies of $Ag3d_{5/2}$ and Ag $3d_{3/2}$ peaks are separated of ca. 6.0 eV, indicating the presence of metallic Ag3d state of silver in as prepared NPs (Zanna et al., 2010). These observations are in good agreement with the XRD results (Fig. 6A).

3.1.6. Extraction of rhein-9-anthrone from sennoside A

The rhein-9-anthrone was formed through bacterial degradation of sennosides A in the colon (Sasaki, et al., 1979). Sennoside A, anthraquinone glycoside is water soluble due to the presence two β-D-glucopyranosyloxy groups. Borntrager's reaction was used for the extraction of rhein-9-anthrone from sennoside A. In a typical experiment, 0.1 g of sennoside A was dissolved in 20 ml double distilled water. Standard HCl (5 ml of 2 M) was added to the as prepared sennoside A extract. To the complete hydrolysis of glycoside linkage, the solution was heated on boiling water bath for 30 min, cooled at room temperature and filtered. The 10 ml $CHCl_3$ was added to the filtrate and shaken. The lower $CHCl_3$ layer was separated and treated with 10% KOH solution. Finally, the upper aqueous layer became red (λ_{max} = 514 nm; Fig. 7), indicating the conversion of sennoside A into rhein-9-anthrone. The complete systematic analysis procedure is summarized in Scheme 5.

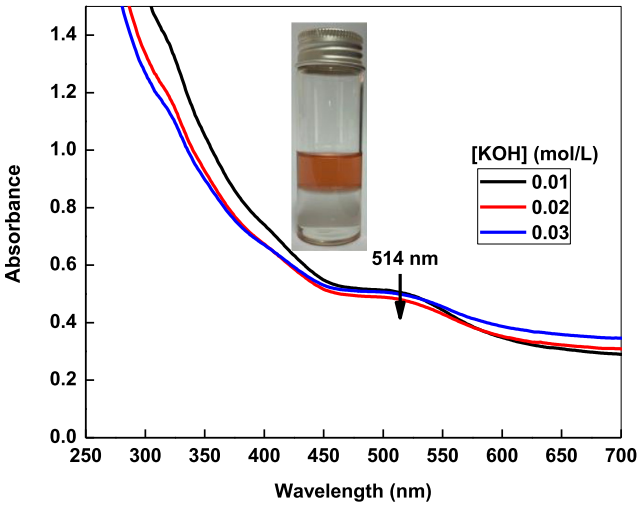

Fig. 7. UV–visible spectra of extracted rhein-9-anthrone in an aqueous alkaline solution.

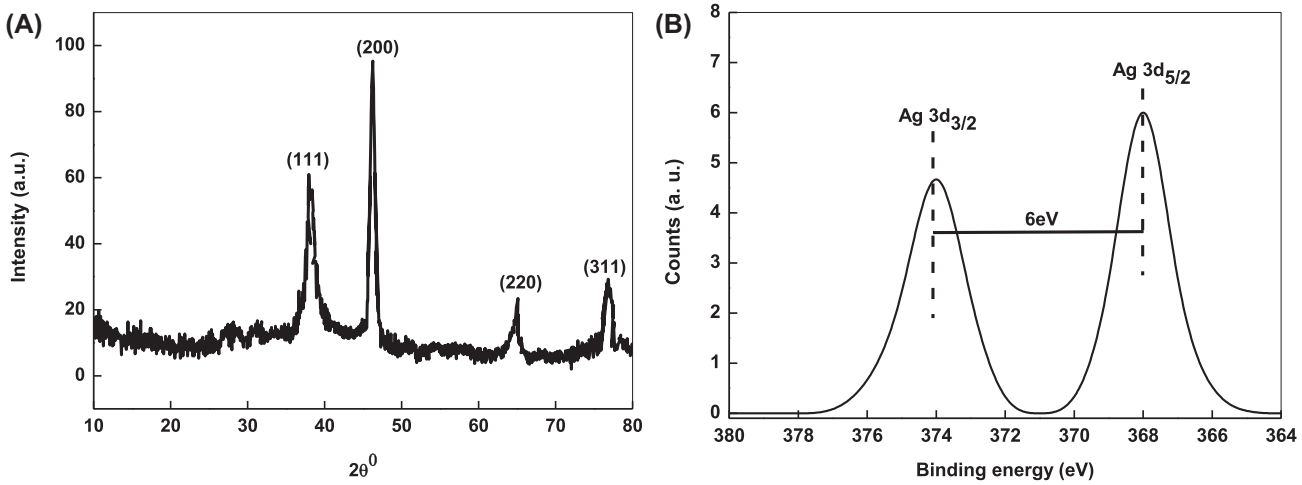

Fig. 6. XRD (A) and XPS (B) spectra of Ag/sennoside A NPs (Ag3d signals).

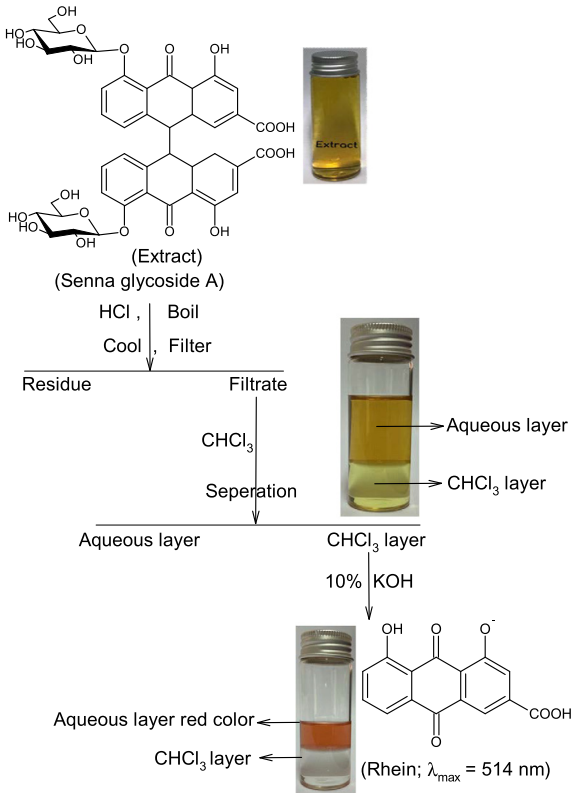

Scheme 5. Systematic extraction of rhein-9-anthrone from an aqueous extract of sennoside A.

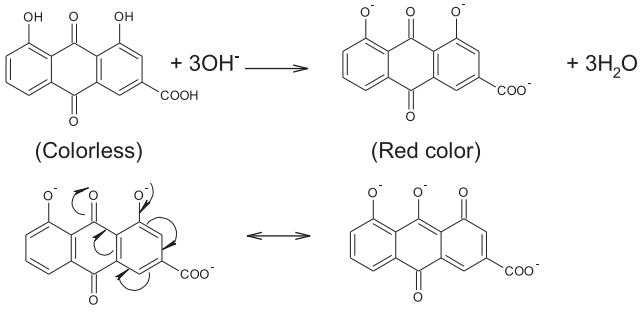

Scheme 6. Stabilization of rhein-9-anthrone in an aqueous alkaline solution.

The rhein-9-anthrone is soluble in $CHCl_3$ and insoluble in water. The aqueous layer of $CHCl_3$- alkaline KOH solution became red color, indicating the formation of water soluble rhein-9-anthrone salt. The appearance of red color might be due to the stabilization of resulting salt via extending conjugation (Scheme 6).

On the other hand, red color of rhein-9-anthrone was decomposed in an aqueous solution slowly and became colorless within a week at 26 °C (Scheme 7), which limits its use for pharmacological investigations (Grimminger and Leng-Peschlow, 1988).

However, the Ag^+ ions (=0.7 × 10^{-3} mol/L) and CTAB (=12.5 × 10^{-4} mol/L) were added into the red color of extracted rhein-9-anthrone. No SPR band of Ag^0 was observed in the UV–visible spectrum, suggested that alkaline solution of rhein-9-anthrone did not acted as a reducing agent. On the basis of above results and discussion, the mechanism of glycosidic bond of sennoside A hydrolysis is proposed in Scheme 8 under acidic conditions.

In Scheme 8, Eq. (8) represents the protonation of glycosidic bond of sennoside A. In the next step (rate determining step; Eq. (9)), glycosidic bonds were broken and rhein-9-anthrone was formed along with the unstable corresponding carbocation, which rapidly converted into the stable product, i.e., D-glucose (Eq. (10)).

3.2. 3.2. Biological aspects

3.2.1. Antioxidant activities

For the biomedical application of NPs, it is essential to determine the accurate molar concentration of NPs in solution (Khlebtsov, 2008). The concentration of Ag/Sennoside A NPs was calculated with the following relation (Sriram et al., 2010) by assuming 100% reduction of Ag^+ ions into Ag^0.

$$N = \frac{\pi \rho N_A}{6M} \times D^3 \tag{11}$$

where N = number of silver atoms per NPs, ρ = density of face centered cubic silver = 10.5 g/cm^3, N_A = 6.02 × 10^{23} (Avogadro's number), M = atomic weight of silver (107.86 g) and D = average diameter of NPs calculated by TEM analysis = 1.2 × 10^{-6} cm. The value of N (=5.3 × 10^4) was calculated by substituting the all parameters in Eq. (11). The molar concentration of NPs solution was determined by using Eq. (12).

$$C = \frac{N_T}{NVN_A} \tag{12}$$

where C = molar concentration of NPs solution, N_T = total number of silver atoms added as metal salt precursor ($AgNO_3$) = 0.1 mol/L, N = 5.3 × 10^4 calculated from Eq. (11), V = volume of reaction solution (0.02 L) and N_A = 6.02 × 10^{23}. The C was found to be 9.4 × 10^{-5} mol/

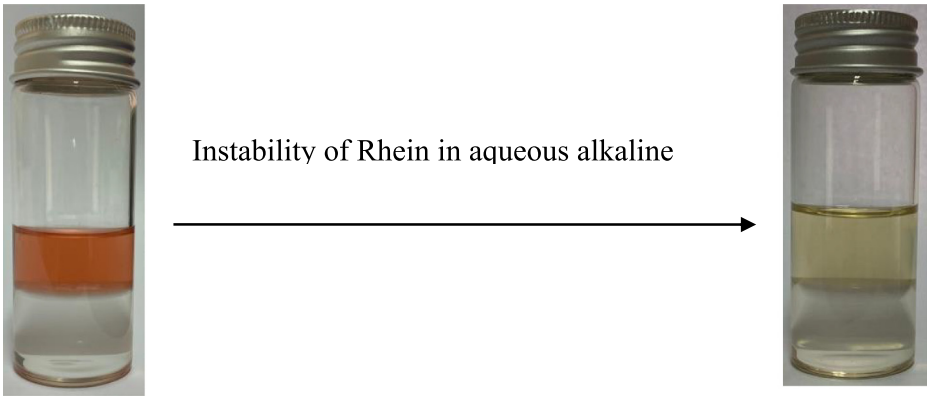

Scheme 7. Instability of rhein-9-anthrone pink color in an aqueous alkaline solution.

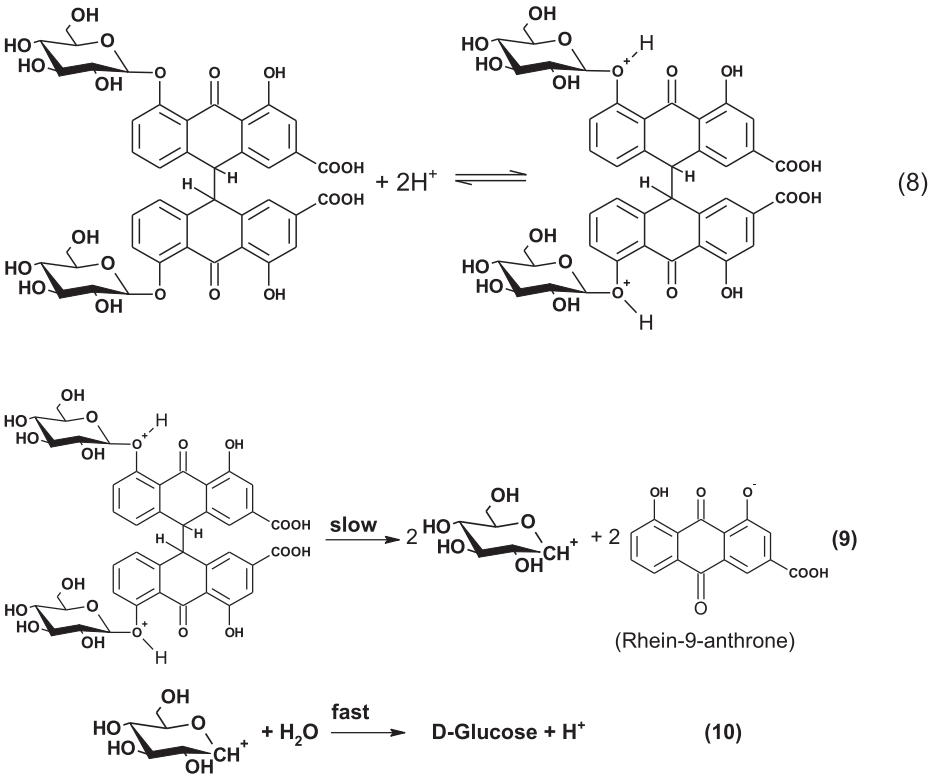

Scheme 8. Hydrolysis of glycosidic bond of sennoside A.

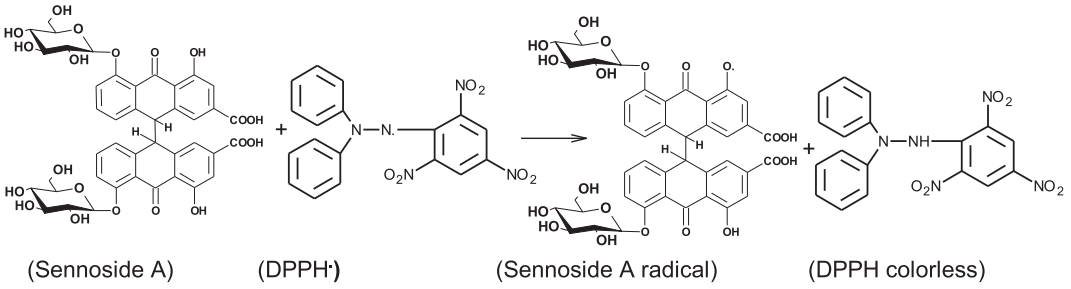

Scheme 9. Antioxidant activity of sennoside A with DPPH radical.

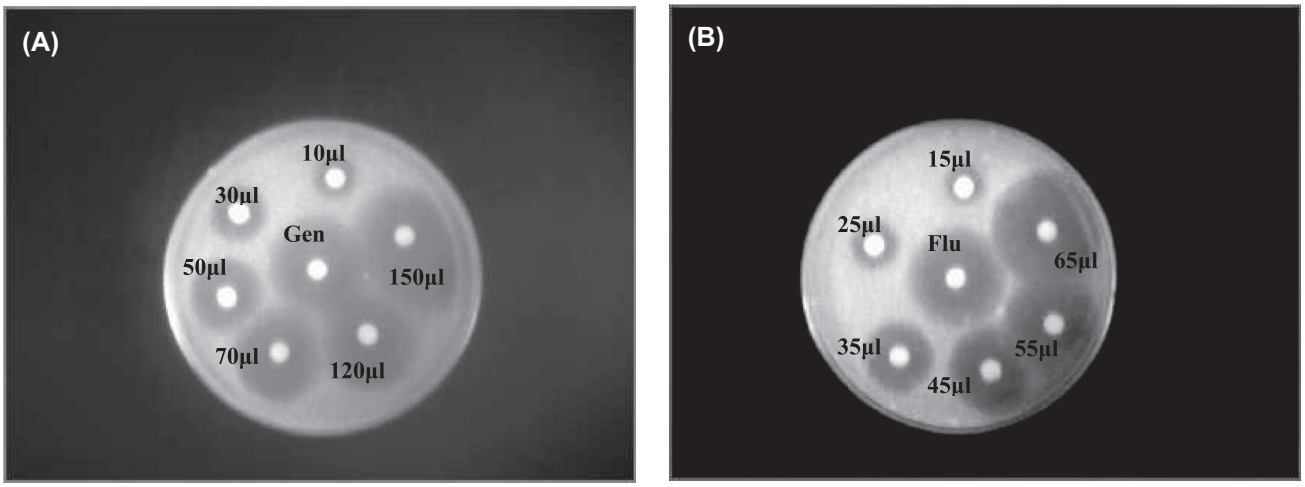

Fig. 8. Disk diffusion assay of Ag/sennoside A NPs against S. aureus (A) and candida albican 10231 (B).

L. The required concentration of each diluted solution may be calculated from this initial concentration according to their relative concentration.

The natural pigments and polyphonols were responsible for the antioxidant properties due to the presence of phenolic –OH groups. The sennoside A and rhein-9-anthrone were used in medicinal and food industries. Antiradical activities of sennoside A and Ag/sennoside A NPs and rhein-9-anthrone were determined against DPPH radical by using UV–visible spectroscopy. For DPPH radical, IC_{50} value was evaluated from the plot of inhibition percentage versus sennoside A concentration. The IC_{50} = 49.5, 46.2 and 53.2 μg /L $DPPH^{\cdot}$ were determined for sennoside A, AgNPs and rhein-9-anthrone, respectively. Antiradical or antioxidant activities of phenolic compounds depend on the transfer of labile H- atom to $DPPH^{\cdot}$. The hydroxyl group (–OH) of sennoside A and rhein-9-anthrone were responsible for the antiradical activity with DPPH radical (Scheme 9 for sennoside A).

3.2.2. Antimicrobial activities

The sennoside A, Ag/sennoside A NPs, and rhein-9-anthrone were screened for their antimicrobial properties against human pathogens by using disk-diffusion method (Nowak et al., 2014). The obtained data, photo of diffusion zone is given in Fig. 8 (A and B for S. aureus and candida albicans) for sennoside A capped AgNPs. The inhibition percentage was calculated by using following Eq. (13).

$$\%\,inhibition = \frac{100 \times (Ag/sennosideA\ inhibition\ area - solvent\ inhibition\ area)}{standard\ drug\ inhibition\ area - solvent\ inhibition\ area} \quad (13)$$

The inhibition area of each experiment was calculated with Eq. (14).

$$Area = \pi r^2 \quad (14)$$

where r = radius of the zone inhibition and π = 3.14. The observed results are depicted graphically in Fig. 9A, B and C as % inhibition against the concentrations of sennoside A, Ag/sennoside A NPs, and rhein-9-anthrone, respectively, which indicated that the inhibition % significantly increases with increasing the concentrations of sennoside A, AgNPs and rhein-9-anthrone. The sizes of the zones inhibition were calculated produced by AgNPs for anti-bacterial S. aureus against gentamicin ranged from 7, 10, 15, 18, 20 and 24 mm for [AgNPs] = 1.0, 3.0, 5.0, 7.0, 12.0 and 15.0 × 10^{-5} mol/L, respectively. For antifungal activities, the zones of inhibition were found to be 5, 8, 14, 16, 20, and 22 mm for [AgNPs] = 1.5, 2.5, 3.5, 4.5, 5.5 and 6.5 × 10^{-5} mol/L, respectively. These findings indicated that the diameter of zone inhibition increases with increasing AgNPs concentrations. Table 2 clearly showed that the inhibition zone diameter produced by AgNPs is higher than that of sennoside A, indicating the combined effect of sennoside A and AgNPs were responsible for higher zone of inhibition and larger surface area.

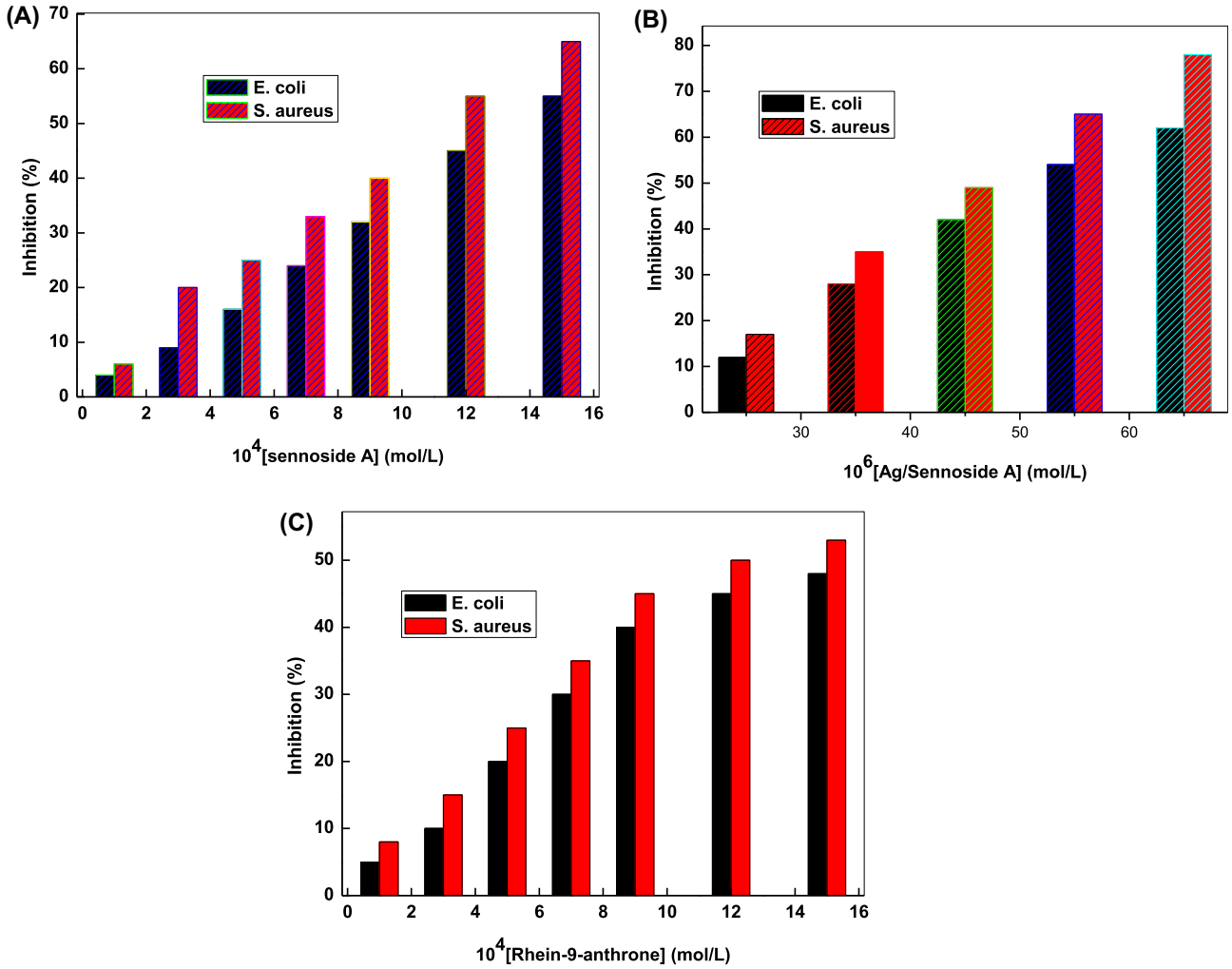

Fig. 9. Effects of sennoside A (A), Ag/sennoside A NPs (B) and rhein-9-anthrone concentrations (C) on the antibacterial activity against E. coli and S. aureus.

Table 2
The results of zone inhibition diameter and surface area of silver NPs antimicrobial test against different human pathogens at 298 K.

Sample	Zone inhibition diameter (mm)			
	E. coli	S. aureus	Albicans10231	Parapsilosis 22019
Sennoside A	8(5.2)[a]	8(5.2)	6(2.8)	5(1.9)
AgNPs	15(17.6)	20(31.4)	22(37.9)	14(15.3)
Gentamicin	22(37.9)	27(57.2)	–	–
Fluconazole	–	–	22(37.9)	25(49.0)

[a] The surface area of inhibition zone was calculated with Eq. (14) are given in the parenthesis in cm.

Khan et al. studied the antimicrobial activities of methanol extract of cassia alata leaves, flowers, stem bark and root bark with different 28 microorganisms and reported that the E. coli and S. aureus were the most active human pathogen (Khan et al., 2001). Our results showed that sennoside A and Ag/sennoside A NPs were most active against with E. coli and S. aureus microorganisms used in this study. The antifungal activities were also determined with candida albicans ATCC 10231 and candida parapsilosis ATCC 22019 under similar conditions (Palanichamy and Nagarajan, 1990). Inspection of Fig. 10 clearly shows that the slopes of inhibition against [sennoside A] are higher in the initial stage, indicating the higher cell death in the first stage. A number of mechanisms have been suggested for the antimicrobial activities of AgNPs by various investigators on several occasions (Sondi and Salopek-Sondi, 2004; Sharma et al., 2009). The release of Ag^+ ions from the surface of AgNPs and reactive oxygen species were responsible for the antimicrobial activities of AgNPs. It is well known that the protein of bacteria cell wall have various coordination sites due to the presence of pH sensitive $-NH_2$, and –COOH groups, which have strong coordinating properties towards metal ions and/or metal NPs. Due to the nano-metric size AgNPs were pass through the cell membrane and formed stable complex with the active functional groups, which disturbed the normal activity of cell well protein, membrane bound enzymes, lipids, DNA replication as well as structure of bacteria. After inclusion of metallic silver in nanoscale into the cell membrane of bacteria, the sulphur containing cysteine oxidized simultaneously and released silver ions into the bacteria (Rahisuddin et al., 2015). The MIC_{50} was found to be 0.63, 0.21,

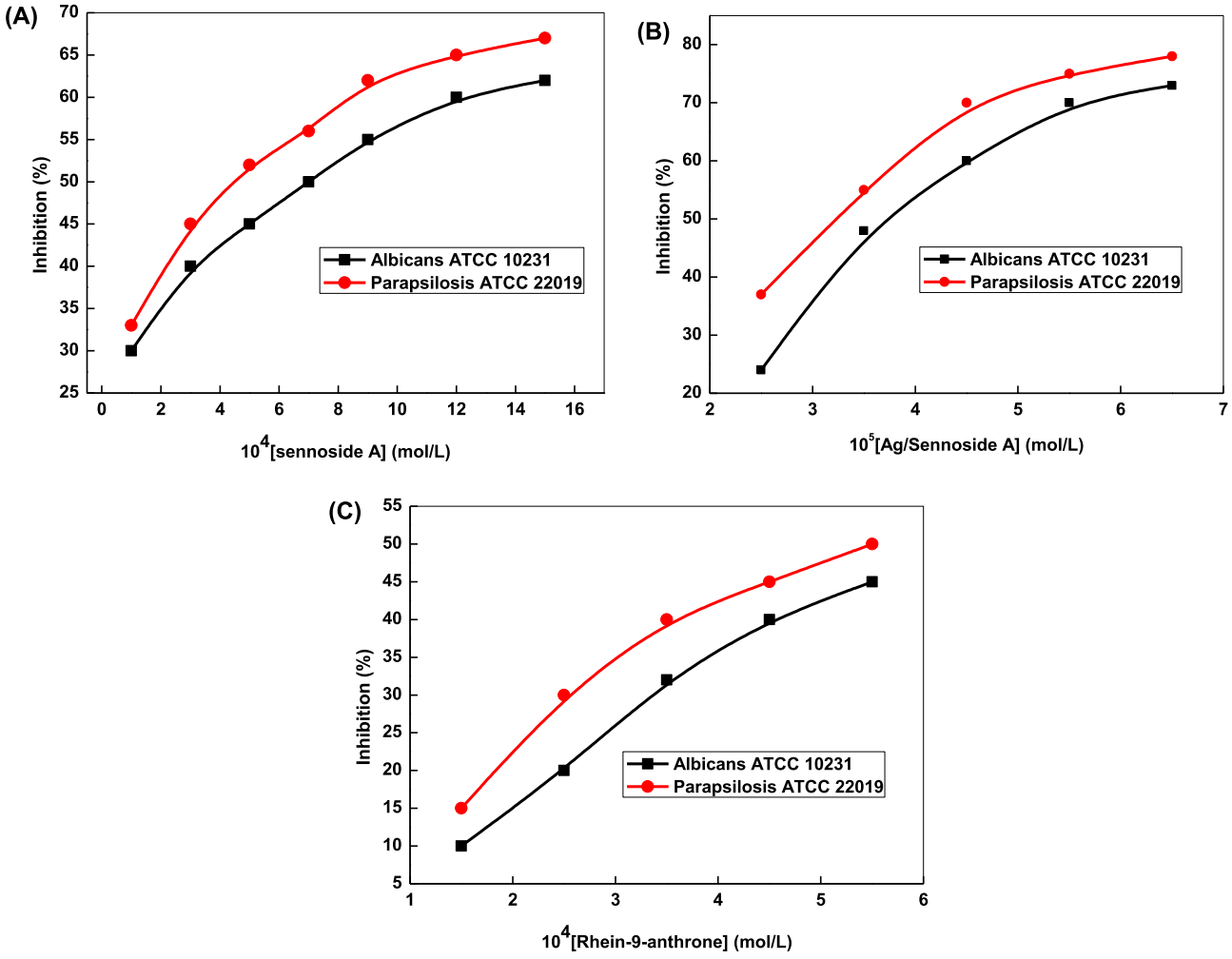

Fig. 10. Growth inhibition percent of candida albicans ATCC 10231 and candida parapsilosis ATCC 22019 as a function of sennoside A (A), Ag/sennoside A NPs and rhein-9-anthrone concentrations (C) on the antifungal activity.

Table 3
Size and shape of AgNPs prepared by using different green plants extract.

Plant's part	Size (nm)	Shapes	Reference
Geranium leafs	16–46	Spherical	Shankar et al. (2003)
Alfalfa sprouts	2–20	Spherical	Gardea-Torresdey et al. (2003)
Caffeine and tea extract	60	Spherical	Nadagouda and Varma (2008)
Olive extract	20–25	Spherical	Khalil et al. (2013)
Palm date fruit	30	Spherical	Zaheer (2018)
Beetroot extract	15	Triangular plate	Kosa and Zaheer (2019)
Walnut shell	25	Spherical	Zaheer (2019)
Zingiber officinale	11–24	Semi-spherical	Eisa et al. (2019)
Henna leafs	1710	Flower like	Bawazir et al. (2020)
Senna leafs	12	Spherical	Present work

0.45 mg/L and 0.53, 0.32, 0. 48 mg/L against antibacterial strain S. aureus and antifungal albicans ATCC 10231 for pure sennoside, Ag/sennoside A NPs, and rhein-9-anthrone, respectively. The excellent inhibitory effect of Ag/sennoside A NPs might be due to the combined synergistic effect of Ag NPs and sennoside A. The incorporation of AgNPs into the cell wall were responsible to inhibit the growth, changes the wall integrity and leads to cell death with the variation of osmotic pressure.

The size of the NPs and PDI markedly influence the antimicrobial activities and other biological application of NPs. The small size NPs and lower PDI are usually shows an excellent activity against human pathogens because they can incorporate easily into the cellular wall, associated with amino acids and disturb the physiological function of the bacteria (Cardoso et al., 2014). The results of present study (small size = 12 nm, lower PDI = 0.6, and negative zeta potential = − 10 mV) showed that the as prepared AgNPs was effective against the bacteria, and fungi, and was a simple, green, economically viable and environmentally friendly green method for the synthesis of AgNPs. The phytochemical, sennoside A also showed antimicrobial activities and responsible for the capping the AgNPs due to the adsorption through its active site.

Scientific literature contained abundant reports regarding the green synthesis of AgNPs by using an aqueous extract of natural plants under different reaction conditions. The morphology of AgNPs strongly depends on the capping nature of biomolecules present in the extract. Some of the reports are summarized in Table 3. Natural plants (leafs, roots, flowers and seeds) were used as a drug to the treatment of human diseases. In the present study, we used sennoside A, extracted from senna leaves (sana makki, valuable herbs of *Tibb-e-Nabwi*, and approved by the Food and Drug Administration as an over-the-counter laxative) extract for the synthesis of AgNPs for the first time. These finding implies that the sennoside A assisted preparation of AgNPs could be an ideal strategy to combat infectious diseases.

4. Conclusion

Sennoside A was extracted from senna leaves extract and endeavoring as a reducing agent to the fabrication of Ag/sennoside A at room temperature. UV–visible data indicates that the optical properties of resulting NPs were dominated by the sennoside A, which formed J-type of aggregates. The controlled morphology of Ag/sennoside A NPs are presented by adjusting the concentration ratio of silver ions to sennoside A in presence of CTAB. The sennoside A and Ag/sennoside A NPs exhibited excellent inhibitory effect against *S. aureus*, *E. coil,* and candida fungus (albicans ATCC 10231 and parapsilosis ATCC 22019), which might be due to the synergistic effect of both metallic silver and sennoside A. Hydrolysis experiments were performed for the isolation of rhein-9-anthrone from sennoside A in alkaline medium. The rhein-9-anthrone was also exhibited antibacterial and antifungal activities against human pathogens. These studies increase the use of sennoside A capped AgNPs and rhein-9-anthrone for the treatment of digestive disorder and anthropoids infection in colon ulcer.

Appendix A. Supplementary material

Supplementary data to this article can be found online at https://doi.org/10.1016/j.jsps.2020.07.003.

References

Abraham, E.P., Chain, E., Fletcher, C.M., Gardner, A.D., Heatley, N.G., Jennings, A.M., Florey, H.W., 1941. Further observations on penicillin. Lancet 2, 177–189.

Ahmad, N., Sharma, S., 2012. Green synthesis of silver nanoparticles using extracts of ananas comosus. Green Sustain. Chem. 2, 141–147.

Bakshi, M.S., 2009. *1D* Flower-like morphologies of palladium nanoparticles using strongly hydrophobic surfactants. J Phys. Chem. C 113, 10921–10928.

Bakshi, M.S., 2016. How Surfactants control crystal growth of nanomaterials. Cryst. Growth Des. 16, 1104–1134.

Bakshi, M.S., 2018. Engineered nanomaterials growth control by monomers and micelles: From surfactants to surface active polymers. Adv. Colloid Interface Sci. 256, 101–110.

Bawazir, W.A., Alhogbi, B.G., Basaleh, A.S., Zaheer, Z., 2020. Capping action of ionic surfactants on the nucleation of lawsone-Ag+ redox system. J. Mol. Liq. 309, 113214.

British Pharmacopoeia, 17th ed., Stationery Office, Department of Health, London, UK, 1999, pp. 1271-1274, 2086-2088.

Brunauer, S., Emmett, P.H., Teller, E., 1938. Adsorption of gases in multi molecular layers. J. Am. Chem. Soc. 60, 309–319.

Cardoso, V.S., Quelemes, P.V., Amorin, A., Primo, F.L., Gobo, G.G., Tedesco, A.C., Mafud, A.C., Mascarenhas, Y.P., Correa, J.R., Kuckelhaus, S.A.S., Eiras, C., Leite, J.R. S.A., Silva, D., Junior, J.R. dos S., 2014. Collagen-based silver nanoparticles for biological applications: synthesis and characterization. J. Nanobiotechnolo. 12, 36–44.

Choi, C., Deng, K.K., Kim, N.-J., Ross Jr, L., Rao, Y.S., Hu, Z., 2008. The inhibitory effects of silver nanoparticles, silver ions, and silver chloride colloids on microbial growth. Water Res. 42, 3066–3074.

Dave, H., Ledwani, L., 2012. A review on anthraquinones isolated from cassia species and their applications. Indian J. Natl. Prod. Resour. 3, 291–319.

Eby, D.M., Luckarift, H.R., Johnson, G.R., 2009. Hybrid antimicrobial enzyme and silver nanoparticle coatings for medical instruments. ACS Appl. Mater. Interfaces 1, 1553–1560

Eisa, W.H., Zayed, M.F., Anis, B., Abbas, L.M., Ali, S.S.M., Mostafa, A.M., 2019. Clean production of powdery silver nanoparticles using Zingiber officinale: The structural and catalytic properties, J. Cleaner Prod. 241, 118398.

Elemike, E.E., Onwudiwe, D.C., Nundkumar, N., Singh, M., Iyekowa, O., 2019. Green synthesis of Ag, Au and Ag-Au bimetallic nanoparticles using Stigmaphyllon ovatum leaf extract and their in vitro anticancer potential. Mater. Lett. 243, 148–152

Gardea-Torresdey, J.L., Gomez, E., Peralta-Videa, J.R., Parsons, J.G., Troiani, H., Jose-Yacaman, M., 2003. Alfalfa sprouts: a natural source for the synthesis of silver nanoparticles. Langmuir 19, 1357–1361.

Grimminger, W., Leng-Peschlow, E., 1988. Instability of rehin-9-anthrone as a problem in pharmacological and analytical use. Pharmacology 36 (suppl. 1), 126–137.

Habib, A.-A.M., Elsebakhy, N.A., 1980. Spectrophotometric estimation of sennosides and rhein glycosides in senna and its preparations. J. Natl. Prod. 43, 452–458.

Haes, A.J., Duyne, R.P.V., 2002. A nanoscale optical biosensor: Sensitivity and selectivity of an approach based on the localized surface plasmon resonance spectroscopy of triangular silver nanoparticles. J. Am. Chem. Soc. 124, 10596–10604.

Hattori, M., Kim, G., Motoike, S., Kobashi, K., Namba, T., 1982. Metabolism of sennosides by intestinal flora. Chem. Pharm. Bull. 30, 1338.

Hayelom, D., Adhena, A., Hailemariam, K., Tekilt, G., 2017. Synthesis paradigm and applications of silver nanoparticles (AgNPs), a review. Sustainable Mater. Technol. 13, 18–23.
Henglein, A., 1993. Physicochemical properties of small metal particles in solution: "microelectrode" reactions, chemisorption, composite metal particles, and the atom-to-metal transition. J. Phys. Chem. 97, 5457–5471.
Henglein, A., 1998. Colloidal silver nanoparticles: Photochemical preparation and interaction with O_2, CCl_4, and some metal ions. Chem. Mater. 10, 444–450.
Henglein, A., 2000. Colloidal palladium nanoparticles: reduction of Pd(II) by H_2; $Pd_{Core}Au_{Shell}Ag_{Shell}$ particles. J. Phys. Chem. B 104, 6683–6685.
Hietala, P., Lainonen, H., Marvola, M., 1988. New aspects on the sennosides. Phramacology 36 (suppl1), 138–143.
Hussain, S., Khan, Z., 2014. Epigallatocatechin-3-gallate capped Ag-nanoparticles: Preparation and characterization. Bioprocess Biosyst. Eng. 37, 1221–1231.
Huy, T.Q., Huyen, P.T.M., Le, A.T., Tonezzer, M., 2019. Recent advances of silver nanoparticles in cancer diagnosis and treatment. Anticancer Agents Med. Chem. https://doi.org/10.2174/1871520619666190710121727.
Khalil, M.M.H., Ismail, E.H., El-Baghdady, K.Z., Mohamed, D., 2013. Green synthesis of silver nanoparticles using olive leaf extract and its antibacterial activity. Arabian J Chem. 7, 1131–1139.
Khan, Z., 2019. Encapsulation of silver nanoparticles into the helix of water soluble starch and their sensing properties. Int. J. Biol. Macromol. 136, 165–176.
Khan, Z., Bashir, O., Hussain, J.I., Kumar, S., Ahmad, R., 2012. Effects of ionic surfactants on the morphology of silver nanoparticles using paan (Piper betel) leaf petiole extract. Colloids Surf. B: Biointerfaces 98, 85–90.
Khan, Z., Khan, M.N., Bashir, O., Khan, T.A., Al-Thabaiti, S.A., 2018. CTAB capped synthesis of bioconjugated silver nanoparticles and their enhanced catalytic activities. J. Mol. Liq. 258, 133–141.
Khan, M.R., Kihara, M., Omoloso, A.D., 2001. Antimicrobial activity of Cassia alata. Fitoterapia 72, 561–564.
Khlebtsov, N.G., 2008. Determination of size and concentration of gold nanoparticles from extinction spectra. Anal Chem. 80, 6620–6625.
Kon, R., Ikarashi, N., Nagoya, C., Takayama, T., Kusunoki, Y., Ishii, M., Ueda, H., Ochiai, W., Machida, Y., Sugita, K., Sugiyama, K., 2014. Rheinanthrone, a metabolite of sennoside A, triggers macrophage activation to decrease aquaporin-3 expression in the colon, causing the laxative effect of rhubarb extract. J. Ethnopharmacol. 152, 190–200.
Kosa, S.A., Zaheer, Z., 2019. Betanin assisted synthesis of betanin@silver nanoparticles and their enhanced adsorption and biological activities. Food Chem. 298, 125014.
Krishnaraj, C., Jagan, E.G., Rajasekar, S., Selvakumar, P., Kalaichelvan, P.T., Mohan, N., 2010. Synthesis of silver nanoparticles using acalypha indica leaf extracts and its antibacterial activity against water borne pathogens. Colloids Surf. B Biointerfaces 76, 50–56.
Mas-Montoya, M., Janssen, R.A.J., 2017. The effect of H- and J-aggregation on the photophysical and photovoltaic properties of small thiophene-pyridine-DPP molecules for bulk-heterojunction solar cells. Adv. Funct. Mater. 27, 1605779.
Meléndrez, M.F., Cárdenas, G., Arbiol, J., 2010. Synthesis and characterization of gallium colloidal nanoparticles. J. Colloid. and Interface Sci. 346, 279–287.
Mueller, S.O., Schmitt, M., Dekant, W., Stopper, H., Schlatter, J., Schreier, P., Lutz, W. K., 1999. Occurrence of emodin, chrysophanol and physcion in vegetables, herbs and liquors, genotoxicity and anti-genotoxicity of the anthraquinones and of the whole plants. Food. Chem. Toxicol. 37, 481–491.
Mulvaney, P., 1996. Surface plasmon spectroscopy of nanosized metal particles. Langmuir 12, 788–800.
Nadagouda, M.N., Varma, R.S., 2008. Green synthesis of silver and palladium nanoparticles at room temperature using coffee and tea extract. Green Chem. 10, 859–862.
Nasiri, J., Rahimi, M., Hamezadeh, Z., Motamedi, E., Naghavi, M.R., 2018. Fulfillment of green chemistry for synthesis of silver nanoparticles using root and leaf extracts of ferula persica: Solid-state route vs. solution-phase method. J. Cleaner Prod. 192, 514–530.
Nowak, R., Olech, M., Pecio, L., Oleszek, W., Los, R., Malmc, A., Rzymowska, J., 2014. Cytotoxic, antioxidant, antimicrobial properties and chemical composition of rose petals. J. Sci. Food Agric. 94, 560–567.
Palanichamy, S., Nagarajan, S., 1990. Antifungal activity of cassia alata leaf extract. J. Ethnopharmacol 29, 337–340.
Paula, V.J.R., Guimaraes, F.M., Diniz, B.S., Forlenza, O.V., 2009. Neurobiological pathways to Alzheimer's disease Amyloid-beta, Tau protein or both?. Dement. Neuropsycho. 3, 188–194.
Rafique, M., Sadaf, I., Rafique, M.S., Tahir, M.B., 2017. A review on green synthesis of silver nanoparticles and their applications. Artificial Cells, Nanomedicine, Biotechnol. 45, 1272–1291.
Rahisuddin, AL-Thabaiti, S.A., Khan, Z., Manzoor, N., 2015. Biosynthesis of silver nanoparticles and its antibacterial and antifungal activities towards gram-positive, gram-negative bacterial strains and different species of candida fungus. Bioprocess Biosyst. Eng. 38, 1773–1781.
Raj, S., Mali, S.C., Trivedi, R., 2018. Green synthesis and characterization of silver nanoparticles using Enicostemma axillare (Lam.) leaf extract. Biochem. Biophys. Res. Commun. 503, 2814–2819.
Raveendran, P., Fu, J., Wallen, S.L., 2003. Completely "green" synthesis and stabilization of metal nanoparticles. J. Am. Chem. Soc. 125, 13940–13941.
Saeb, Amr T.M., Alshammari, Ahmad S., Al-Brahim, Hessa, Al-Rubeaan, Khalid A., 2014. Production of silver nanoparticles with strong and stable antimicrobial activity against highly pathogenic and multidrug resistant bacteria. The Sci. World J. 2014, 1–9. https://doi.org/10.1155/2014/704708.
Sasaki, K., Yamauchi, K., Kuwano, S., 1979. Metabolic activation of sennoside A in mice. Planta Med. 37, 370–378.
Sendelbach, L.E., 1989. A review of the toxicity and carcinogenicity of anthraquinone derivatives. Toxicol. 57, 227–240.
Shankar, S.S., Ahmad, A., Sastry, M., 2003. Geraniumleaf assisted biosynthesis of silver nanoparticles. Biotechnol. Prog. 19, 1627–1631.
Shankar, S.S., Rai, A., Ahmad, A., Sastry, M., 2004. Rapid synthesis of Au, Ag, and bimetallic Au core-Ag shell nanoparticles using neem (Azadirachta indica) leaf broth. J. Colloid Interface Sci. 275, 496–502.
Sharma, V.K., Yngard, R.A., Lin, Y., 2009. Silver nanoparticles: Green synthesis and their antimicrobial activities. Adv. Colloid Interface Sci. 145, 83–96.
Sheny, D.S., Mathew, J., Philip, D., 2011. Phytosynthesis of Au, Ag and Au-Ag bimetallic nanoparticles using aqueous extract and dried leaf of Anacardium occidentale. Spectrochim. Acta A 79, 254–262.
Sondi, I., Salopek-Sondi, B., 2004. Silver nanoparticles as antimicrobial agent: A Case Study on E. Coli as a model for gram-negative bacteria. J. Colloid Interf. Sci. 275, 177–182.
Sun, S.-W., Su, H.-T., 2002. Validated HPLC method for determination of sennosides A and B in senna tablets. J. Pharm. Biomed. Anal. 29, 881–894
Sriram, M.I., Kanth, S.B.M., Kalishwaralal, K., Gurunathan, S., 2010. Antitumor activity of silver nanoparticles in Dalton's lymphoma ascites tumor model. Int. J. Nanomedicine 5, 753–762.
Tan, P., Zhao, Y.-L., Cao, J.-L., Xiao, X.-H., Wang, J.-B., 2015. Development and validation of an ultra-high-performance liquid chromatography for the determination of sennoside A and sennoside B in laxatives based on optimal chromatographic parameters. Anal. Methods 7, 9817–9824.
Thomson, R.H., 1971. Naturally Occurring Quinones. Academic, London.
Tyler, V.E., Brady, L.R., Robbers, J.E., 1988. Pharmacognosy. Lea and Febiger, Philadelphia, PA, USA, p. 65.
van Gorkom, B.A., Karrenbeld, A., van der Sluis, T., Zwart, N., de Vries, E.G., Kleibeuker, J.H., 2001. Apoptosis induction by sennoside laxatives in man; escape from a protective mechanism during chronic sennoside use?. J. Pathol. 194, 493–499.
Wang, X.F., Shen, Y.H., Xie, A.J., Chen, S.H., 2013. One-step synthesis of Ag@PANI nanocomposites and their application to detection of mercury. Mater. Chem. Phys. 140, 487–492.
Wojtysiak, S., Kudelski, A., 2012. Influence of oxygen on the process of formation of silver nanoparticles during citrate/borohydride synthesis of silver sols. Colloids Surf. A: Physicochem. Eng. Aspects 410, 45–51.
Xie, J., Lee, J.Y., Wang, D.I.C., Ting, Y.P., 2007. Silver nanoplates: from biological to biomimetic synthesis. ACS Nano 1, 429–439.
Yen, G.C., Duh, P.D., Chuang, D.Y., 2000. Antioxidant activity of anthraquinones and anthrone. Food. Chem. 70, 437–441.
Zaheer, Z., 2019. Eco-friendly walnut shell powder based facile fabrication of biogenicAg-nanodisks, and their interaction with bovine serum albumin. J. Photochem. Photobiol. B: Biology 193, 8–17.
Zaheer, Z., Aazam, E.S., Kosa, S.A., 2016. Effects of cationic and anionic micelles on the morphology of biogenic silver nanoparticles, and their catalytic activity for congo red. J. Mol. Liq. 220, 364–369.
Zaheer, Z., 2018. Biogenic synthesis, optical, catalytic, and in vitro antimicrobial potential of Ag-nanoparticles prepared using palm date fruit extract. J. Photochem. Photobio., B: Biology 178, 584–592
Zanna, S., Saulou, C., Mercier-Bonin, M., Despax, B., Raynaud, P., Seyeux, A., Marcus, P., 2010. Ageing of plasma-mediated coatings with embedded silver nanoparticles on stainless steel: an XPS and ToF-SIMS investigation. Appl. Surf. Sci. 256, 6499–6505.